JARO 5: 215–226 (2004)
DOI: 10.1007/s10162-003-4020-3

JARO
Journal of the Association for Research in Otolaryngology

Null Mutation of α_{1D} Ca^{2+} Channel Gene Results in Deafness but No Vestibular Defect in Mice

HONGWEI DOU,[1] ANA E. VAZQUEZ,[2] YOON NAMKUNG,[3] HANQI CHU,[2] EMMA LOU CARDELL,[1] LIPING NIE,[2] SUSAN PARSON,[2] HEE-SUP SHIN,[3] AND EBENEZER N. YAMOAH[2]

[1]*Department of Pediatric Otolaryngology, Children's Hospital Medical Center, Cincinnati, OH 45229, USA*
[2]*Center for Neuroscience, Department of Otolaryngology, University of California, Davis, CA 95616, USA*
[3]*National Creative Research Initiatives Center for Calcium and Learning, and Department of Life Science, Division of Molecular and Life Sciences, Pohang University of Science and Technology, Pohang, Korea*

Received: 7 May 2003; Accepted: 21 January 2004; Online publication: 4 May 2004

ABSTRACT

Multiple Ca^{2+} channels confer diverse functions to hair cells of the auditory and vestibular organs in the mammalian inner ear. We used gene-targeting technology to generate α_{1D} Ca^{2+} channel-deficient mice to determine the physiological role of these Ca^{2+} channels in hearing and balance. Analyses of auditory-evoked brainstem recordings confirmed that $\alpha_{1D}{}^{-/-}$ mice were deaf and revealed that heterozygous ($\alpha_{1D}{}^{+/-}$) mice have increased hearing thresholds. However, hearing deficits in $\alpha_{1D}{}^{+/-}$ mice were manifested mainly by the increase in threshold of low-frequency sounds. In contrast to impaired hearing, $\alpha_{1D}{}^{-/-}$ mice have balance performances equivalent to their wild-type littermates. Light and electron microscope analyses of the inner ear revealed outer hair cell loss at the apical cochlea, but no apparent abnormality at the basal cochlea and the vestibule. We determined the mechanisms underlying the auditory function defects and the normal vestibular functions by examining the Ba^{2+} currents in cochlear inner and outer hair cells versus utricular hair cells in $\alpha_{1D}{}^{+/-}$ mice. Whereas the whole-cell Ba^{2+} currents in inner hair cells consist mainly of the nimodipine-sensitive current (~85%), the utricular hair cells express only ~50% of this channel subtype. Thus, differential expression of α_{1D} channels in the cochlear and utricular hair cells confers the phenotype of the α_{1D} null mutant mice. Because vestibular and cochlear hair cells share common features and null deletion of several genes have yielded both deafness and imbalance in mice, α_{1D} null mutant mice may serve as a model to disentangle vestibular from auditory-specific functions.

Keywords: hearing, balancing, inner ear, hair cells, Ca^{2+} channels, voltage clamp

INTRODUCTION

Despite the general agreement that distinct voltage-gated Ca^{2+} channels serve as the principal conduits for Ca^{2+} influx into cells, thus conferring specific Ca^{2+}-dependent functions, the exact role(s) of individual Ca^{2+} channel subtypes remains largely unknown. Even for specific functions such as neurotransmitter release, neurons employ more than one type of Ca^{2+} channel to execute this function, suggesting substantial redundancy in the nervous system (Smith and Cunnane 1997; Wu et al. 1999). There are three families of voltage-gated Ca^{2+} channels (VGCCs) with intrafamily sequence identities above 80% (Ertel et al. 2000) and additional diversity is generated by alternative splicing of exons encoding the cytoplasmic loop of different repeats of the α subunits (Solatov et al. 1995; Lin et al. 1997; Kollmar et al. 1997a, b). Genes for the voltage-gated channel $Ca_V1.3$ (α_{1D}) are expressed throughout the

Correspondence to: Ebenezer N. Yamoah • University of California, Davis • Center for Neuroscience • Department of Otolaryngology • 1544 Newton Court • Davis, CA 95616 • Telephone: (530) 754-6630; Fax: (530) 754-5046; email: enyamoah@ucdavis.edu

nervous system and play a minor role in neurotransmitter release (Wu et al. 1999; Ertel et al. 2000). In hair cells, however, the channel is the most abundant isoform (Zidanic and Fuchs 1995; Rodriguez–Contreras and Yamoah 2001, 2002), suggesting distinct physiological roles in the inner ear.

Hair cells form a tonic synapse with afferent nerve terminals of the eighth cranial nerve and are poised to respond rapidly to sustained stimuli of different intensities and to transmit amplitude and frequency modalities of the stimuli (Hudspeth 1989). The fast neurotransmitter release in hair cells relies on the voltage- and time-dependent properties of clusters of α_{1D} Ca^{2+} channels at the release sites (Rodriguez–Contreras and Yamoah 2001; Rispoli et al. 2001). Moreover, the whole-cell current activates at low membrane voltages (~−50 mV), has a fast activation time constant (~0.5 ms), and has half-activation voltages ranging from −40 to +20 mV (Hudspeth and Lewis 1988; Zidanic and Fuchs 1995; Martini et al. 2000; Platzer et al. 2000; Rodriguez–Contreras and Yamoah 2001). Furthermore, hair cells may express not only α_{1D} Ca^{2+} channels alone, but several other distinct Ca^{2+} channels as well, ensuring multiple Ca^{2+}-dependent processes. The differential roles of distinct Ca^{2+} channel subtypes in hair cells have been proposed using evidence from immunocytochemical, polymerase chain reaction (PCR), and electrophysiological techniques. Variants of $Ca_V1.2$ (α_{1C}), $Ca_V2.2$ (α_{1B}), and $Ca_V2.3$ (α_{1E}) have been localized in cochlear and other hair cells (Green et al. 1996; Lopez et al. 1999; Rodriguez–Contreras and Yamoah 2001).

To analyze the physiological role of α_{1D} Ca^{2+} channels in hair cells, we used gene targeting to produce α_{1D}-deficient mice. The results of our analyses demonstrate that α_{1D} is crucial for hearing, but less so for maintaining balance.

METHODS

Generation of α_{1D}-deficient mice

Conventional gene-targeting technology was used to generate Ca^{2+} channel α_{1D} null mutant mice (Namkung et al. 2001). A murine $Ca_V1.3$ genomic DNA clone having the first two exons of the gene was isolated from a 129/SVJ mouse genomic library. The region extending from half of the 3′ part of the first exon to half of the 5′ part of the second exon was deleted and replaced by the IRES β-gal expression cassette and the NEO cassette. The negative selection marker, TK cassette, was inserted into the end of the 3′ homology region of the targeting vector. The targeting vector was transfected into J1 embryonic stem (ES) cells. Chimeras were backcrossed to C57BL/6J mice. Germline transmission was determined by DNA typing of tail DNA. $\alpha_{1D}^{+/-}$ mice were then intercrossed to obtain $\alpha_{1D}^{-/-}$ mice. All mice analyzed were from F2 and F3 generations. Because the $\alpha_{1D}^{-/-}$ mice were fertile, they were further intercrossed to increase the sample number of null mutants.

Gross evaluation of auditory and vestibular functions

We evaluated the ear twitch response of ten wild-type $\alpha_{1D}^{+/+}$, $\alpha_{1D}^{+/-}$ and $\alpha_{1D}^{-/-}$ mice with a hand clap (Preyer's reflex) to grossly assess the hearing status of the three genotypes. To obtain a gross assessment of the vestibular (utricular) function of the mice, we performed a swim test. Mice were placed in a water bath at 37°C and allowed to swim and climb onto a dry platform. The swimming performance and the time taken to swim to the target were scored in a blind fashion. Seven $\alpha_{1D}^{+/+}$ and $\alpha_{1D}^{-/-}$ mice each were tested. Balance was further tested using a custom-made setup as described by Xiang et al. (1997). Mice were placed on a soft fabric-covered horizontal cylinder (~7 cm in diameter) and positioned 10 cm above a foam pad. The cylinder was connected to a variable speed motor that runs from 0 to 15 rpm. Each animal's ability to balance on both the stationary cylinder and the rotating cylinder was scored. Seven $\alpha_{1D}^{+/+}$ and $\alpha_{1D}^{-/-}$ mice each were tested.

Auditory brainstem responses

Twenty $\alpha_{1D}^{+/+}$, 28 $\alpha_{1D}^{+/-}$, and 19 $\alpha_{1D}^{-/-}$ mice (age range: 5–8 weeks old) were anesthetized with avertin and auditory brainstem response (ABR) measurements were recorded as previously described (Kozel et al. 1998; Flagella et al. 1999). Briefly, a ground needle electrode and recording needle were placed subcutaneously in the scalp, and then a calibrated electrostatic speaker coupled to a hollow ear bar was placed inside the pinna. Broadband clicks and pure tones (8, 16, and 32 kHz) were presented in the animal's ear in 10 dB increments, starting from 0 dB SPL and ending at 100 dB SPL. The ABR sweeps were computer-averaged (time-locked with onset of 128–1024 stimuli, at 20/s) out of the continuous electroencephalographic activity. The threshold of hearing was determined as the lowest intensity of sound required to elicit a characteristic waveform.

Light microscopy of the inner ear

Light microscope analyses of the cochlea and vestibular organs of the inner ear from 5–12-week-old mice of all genotypes were studied using procedures

described in Kozel et al. (1998). The mice were deeply anesthetized with sodium pentobarbital and transcardially perfused with a solution containing 2% glutaraldehyde and 2% paraformaldehyde in 0.1 M cacodylate buffer, pH 7.3. The temporal bones were harvested and the inner ears were perfused with fixative through the oval and round windows and left in fixative overnight. The temporal bones were decalcified in a 0.1 M EDTA solution for 1 week. The specimens were postfixed in buffered 1% osmium tetroxide (OsO_4) for 1–2 h at room temperature, dehydrated in graded ethanol solutions followed by propylene oxide, and embedded in Spurr's resin. Serial sections (1–2 μm) parallel to the modiolus of the inner ears were cut and stained with toluidine blue and then subsequently coverslipped.

Scanning electron microscopy of the inner ear

Five mice from each genotype were selected for scanning electron microscope analyses. Similar to the procedures for light microscopy, the temporal bones were harvested and fixed in 2% glutaraldehyde in 0.1 M phosphate buffer saline (PBS) for 36 h at room temperature (~21°C) and decalcified in 0.1 M EDTA for 5 days. The cochlea, utricle, saccule, and the semicircular canals were dissected out of the specimen and postfixed in 1% OsO_4 for 2 min. Dehydration of the specimen was carried out in a graded ethanol series. The specimens were critical-point dried from liquid CO_2, sputter-coated with gold–palladium, and examined in a scanning electron microscope (Philips XL30). Digital images were captured and stored in a personal computer interfaced with the microscope.

Distortion product otoacoustic emissions (DPOAE)

Mice were anesthetized with ketamine (95 mg/kg) and xylazine (4 mg/kg). The f_1 and f_2 primary tones were generated by a 2-channel frequency synthesizer (Hewlett Packard 3326A), presented over two tweeters (Realistic), and delivered through a small soft rubber probe tip. Ear-canal sound pressure was measured with a commercial acoustic probe (Etymotic Research 10B$^+$). The ear-canal sound pressure was sampled and synchronously averaged (n = 8) by a digital signal processor for frequencies <20.1 kHz, and by a dynamic signal analyzer (Hewlett Packard 3561A) for frequencies >20.1 kHz. DF-grams were collected over a range of geometric mean frequencies between 5.6 and 48.5 kHz (f_2 = 6.3–54.2 kHz), in 0.5-octave intervals at stimulus levels of $L_1 = L_2$ = 65 dB SPL, with f_2/f_1 = 1.25.

Whole-cell recording of Ba^{2+} currents

Standard patch-clamp recording techniques were used to record whole-cell currents to study the Ba^{2+} currents in cochlear and utricular hair cells in intact sensory epithelia. Utricles and cochleae were excised from young wild-type (+/+) and homozygous mutant (−/−) mice between postnatal days 1–10, as described in previous reports (Rüsch and Eatock 1996; Holt et al. 1997; Moser and Beutner 2000). All chemicals were obtained from Sigma Chemical Co. (St Louis, MO), unless indicated. Mice were sacrificed by cervical dislocation and decapitation. The sensory epithelium was removed from each inner ear while immersed in MEM solution (GIBCO, pH 7.4 with 10 mM HEPES: Gaithersburg, MD). The bony labyrinth was opened, and once the epithelium of interest was exposed, the tissue was treated with protease XXVII (100 μg/ml, 15 min). The surrounding extraneous tissue and nerve were trimmed away and the sensory epithelium was then mounted on a recording chamber with Cell-Tak (Collaborative Biomedical Products, Bedford, MA). The mounted epithelia were placed under an upright Olympus compound microscope (IX50). Solutions used in the experiments were as follows with mM quantities of each component given: Modified Tyrode, consisting of 130 Na^+, 3 K^+, 4 Ca^{2+}, 5 glucose, and 5 HEPES, pH 7.4 (NaOH). The external solution for recording Ba^{2+} current contained 105 Na^+, 25 TEA, 5 4-AP, 1 Ba^{2+}, 5 HEPES, and 5 glucose. The patch-pipette filling solution contained 80 NMG, 40 Cs^+, 1 Mg^{2+}, 5 EGTA, 10 HEPES, 3 ATP, 1.5 GTP, pH 7.4 (CsOH). Thus, outward K^+ currents were suppressed with 4-AP, TEA, Cs^+, and the nonpermeant cation NMG. Stock solutions of Bay K 8644 (Bay K: Calbiochem, La Jolla, CA) and nimodipine (Calbiochem) were dissolved in 100% dimethyl sulfoxide (DMSO). The final concentrations of Bay K and nimodipine were 10 and 20 μM, respectively.

Patch-pipettes (1.5 mm o.d. and 1 mm i.d.) were pulled from borosilicate glass using the horizontal puller, P87 (Sutter Instrument, Novato, CA). Patch electrodes had 2–5-MΩ tip resistances when filled with the pipette solution. Recordings were done using an Axopatch 200B patch-clamp amplifier interfaced with a personal computer equipped with pClamp software (Axon Instruments, Foster City, CA). Currents were filtered at 2 kHz and sampled at 10 kHz. Leakage and capacity currents were subtracted using the p/4 method. Data analyses were performed using the pClamp and Origin software (MicroCal Inc., Northampton, MA). Where appropriate, pooled data were presented as means ± SD. Significant differences between groups were tested using Student's t-test [data with $p > 0.05$ were considered not significant (NS)].

RESULTS

Hearing defect and normal balance in $\alpha_{1D}^{-/-}$ mice

The gene encoding the murine α_{1D} Ca^{2+} channel was deleted and replaced with the IRES β-gal expression and NEO cassettes in a manner described recently (Namkung et al. 2001). Consistent with auditory phenotypes of α_{1D} null mutant mice reported by Platzer et al. (2000), the homozygous mutant mice showed no motor response to auditory stimuli (Preyer's test) which is suggestive of hearing impairment. To test the hypothesis that null deletion of α_{1D} Ca^{2+} channels might alter hearing sensitivity, ABRs were analyzed to determine the sound pressure levels at which typical ABR waveforms could be detected. The wild-type mice exhibited the characteristic ABR waveform beginning at sound pressure levels of ~30, 25, 10, and 16 dB using broadband clicks and pure tones of 8, 16, and 32 kHz stimuli (Fig. 1A). The $\alpha_{1D}^{+/-}$ yielded elevated thresholds for broadband clicks and 8 and 16 kHz pure tones (mean threshold; clicks: $\alpha_{1D}^{+/+} = 34 \pm 5$ dB ($n = 20$), $\alpha_{1D}^{+/-} = 44 \pm 7$ dB ($n = 28$), $p < 0.01$; 8 kHz: $\alpha_{1D}^{+/+} = 26 \pm 6$ dB ($n = 20$), $\alpha_{1D}^{+/-} = 31 \pm 7$ dB ($n = 28$), $p < 0.05$; 16 kHz: $\alpha_{1D}^{+/+} = 7 \pm 4$ dB ($n = 20$), $\alpha_{1D}^{+/-} = 11 \pm 6$ dB ($n = 28$), $p < 0.01$. However, at 32 kHz, the thresholds for ABR waveforms were not significantly different (mean threshold; 32 kHz: $\alpha_{1D}^{+/+} = 16 \pm 6$ dB ($n = 20$), $\alpha_{1D}^{+/-} = 18 \pm 6$ dB ($n = 28$), $p = 0.3$ NS: Fig. 1B). In contrast, all $\alpha_{1D}^{-/-}$ mice ($n = 19$) exhibited no response as measured by ABR, even up to the maximum sound pressure level (100 dB) of acoustic stimulation (Fig. 1A).

Because α_{1D} Ca^{2+} channels are expressed in hair cells in the inner ear (Green et al. 1996; Lopez et al. 1999), we also performed gross assessment of the vestibular phenotype of mutant mice compared with their age-matched littermates. We utilized two quantitative tests: first, setting criteria for time required to swim to a dry platform and, second, for the mice to balance on both a stationary and a rotating cylinder (Fig. 2A, B). As shown in Figure 2C, $\alpha_{1D}^{+/+}$ and $\alpha_{1D}^{-/-}$ mice yielded similar scores for the swim and balance tests. The apparent lack of balance deficit implied normal functioning of both the utricle and semicircular canals, even in the absence of α_{1D} Ca^{2+} channels.

Histology of the inner ear

In adult $\alpha_{1D}^{+/+}$ mice, the organ of Corti consists of an arrangement of 3 rows of outer (OHC) and 1 row of inner (IHC) hair cells bearing highly organized and tall stereocilia bundles. These hair cells, in turn, are flanked by the supporting cells covered with shorter irregular microvilli. To determine if null deletion of α_{1D} Ca^{2+} channels altered the morphology of hair cells, the organ of Corti was exposed by removing the tectorial membrane and examined by scanning electron microscopy (Fig. 3). In $\alpha_{1D}^{+/+}$ mice, the organ of Corti showed normal architecture of the row of IHCs and OHCs along the apical (Fig. 3A) and basal (Fig. 3C) turns of the cochlea. In contrast, the apical turn of the organ of Corti in $\alpha_{1D}^{-/-}$ mice was devoid of typical rows of stereociliary bundles, with the apical modifications consisting instead of scattered patches of hair bundles and flanking sheets of supporting cells (Fig. 3C). Hair bundles of the IHCs remained normal in all turns of the cochlea in both $\alpha_{1D}^{+/+}$ and $\alpha_{1D}^{-/-}$ mice (Fig. 3A–D). Moreover, at the basal turn of the cochlea, the $\alpha_{1D}^{-/-}$ mice appear to have morphologically intact OHCs (Fig. 3D). These findings are in sharp contrast with earlier reports that indicated complete degeneration of IHCs and OHCs in 5-week-old $\alpha_{1D}^{-/-}$ mice. (Platzer et al. 2000) based on light microscopy analysis alone. Although there appears to be gradual degeneration of hair bundles of OHCs extending to the base of the cochlea in an age-dependent manner in the $\alpha_{1D}^{-/-}$ mice, we continued to observe intact OHCs at the basal turn of the cochlea even in 15-week-old homozygous mutant mice (data not shown). Direct comparison of the $\alpha_{1D}^{-/-}$ and $\alpha_{1D}^{+/+}$ mice was complicated by the fact that the background C57BL/6J wild-type mice experienced age-induced hearing loss beginning at ~12 weeks, accompanied by OHC loss at the basal turn (Henry and Chole 1980). Nonetheless, it is clear from our studies that the effects on OHC morphology induced by α_{1D} Ca^{2+} channel deletion were mostly restricted to the apex of the cochlea. Consistent with the lack of a balance defect in the $\alpha_{1D}^{-/-}$ mice, the hair bundles of the utricle (Fig. 3E, G) and saccule (Fig. 3F, H) were morphologically indistinguishable from those of the $\alpha_{1D}^{+/+}$ mice.

Degeneration of hair bundles of OHCs at the apical turn may represent an isolated and local defect. However, the absence of characteristic ABR waveforms in $\alpha_{1D}^{-/-}$ mice (Fig. 1) could signify a general alteration of cochlear structure. To disentangle these possibilities, 2-μm serial sections of the inner ear stained with toluidine blue were analyzed. The panels in Figure 4 show that the cochlear ducts of 6-week-old $\alpha_{1D}^{-/-}$ mice exhibit no aberrations in the overall organ of Corti architecture, in the partitioning by the Reissner's membrane (RM), or in the stria vascularis (StV) morphology. They do, however, differ from $\alpha_{1D}^{+/+}$ cochlea in the absence of tufts of hair bundles at the apical turn; note that the cell bodies of OHCs can be clearly seen at the apical (Fig. 4A, D) as well as the basal (Fig. 4C, F) turns in wild-type and mutant cochleae. Another difference observed in the

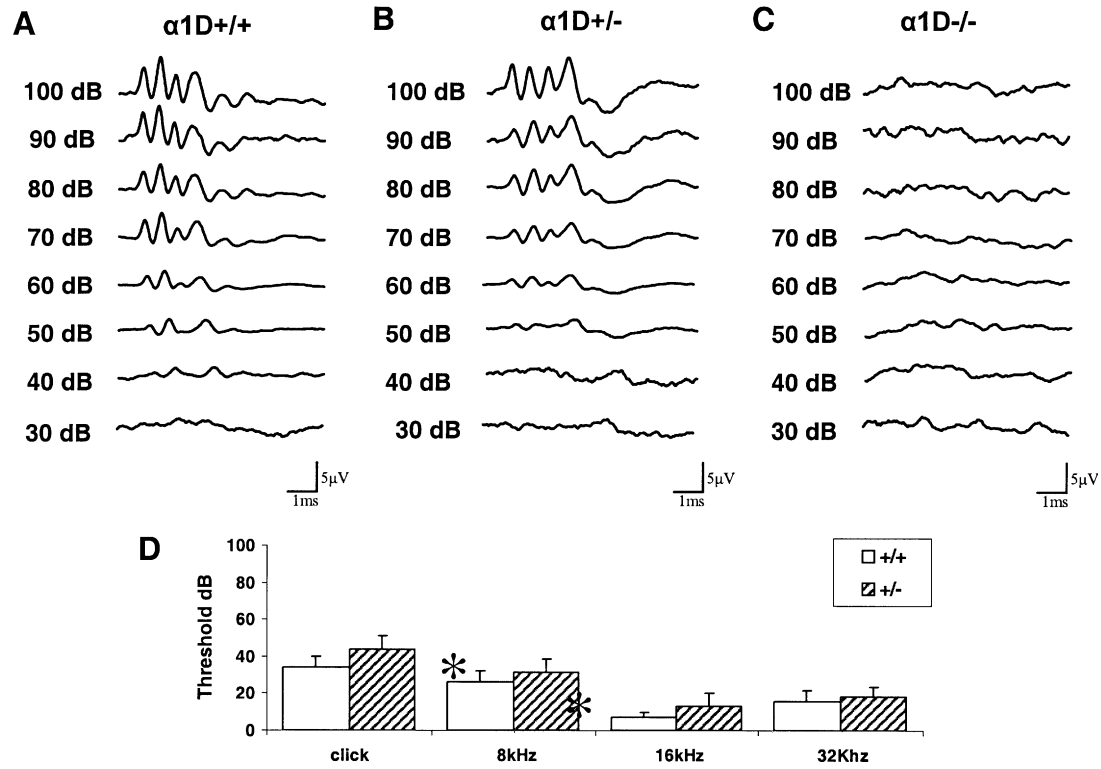

FIG. 1. ABR thresholds from the right ears of wild-type (**A**), heterozygous (**B**), and homozygous (**C**) mice (5–8 week old). The sound pressure levels in dB of broadband clicks (0.1 ms) delivered to the ear are indicated on the left side of the traces. Representative normal broadband click responses from $\alpha_{1D}^{+/+}$ mice are shown; the heterozygous mice $\alpha_{1D}^{+/-}$ showed increased threshold. No response was observed from any of the 19 $\alpha_{1D}^{-/-}$ mice examined. **D**. ABR thresholds for $\alpha_{1D}^{+/+}$ ($n = 20$) and $\alpha_{1D}^{+/-}$ ($n = 28$) mice in response to broadband clicks and 3-ms pure tones of 8, 16, and 32 kHz ($p < 0.05$ at 8 and 16 kHz and $p = 0.3$ at 32 kHz). The asterisks denote the comparisons, which are statistically significant. The data are means ± SD.

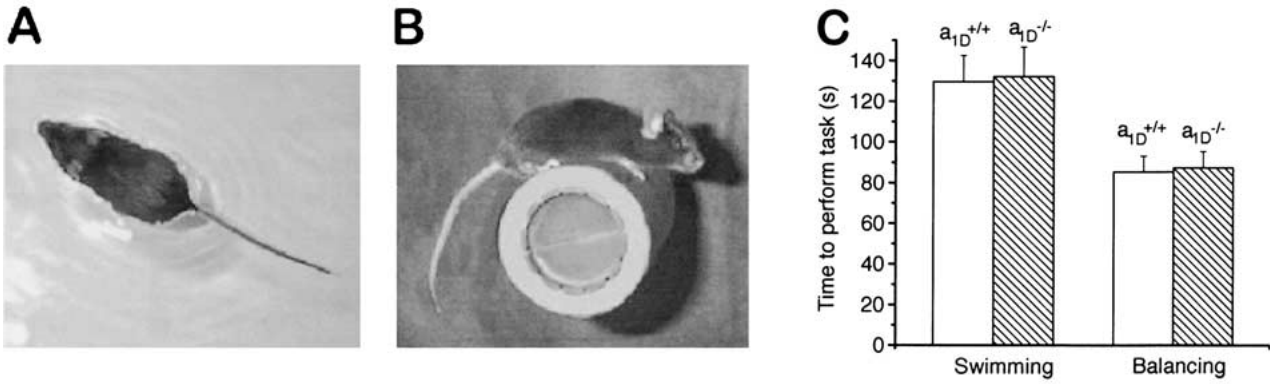

FIG. 2. α_{1D} Ca^{2+} channel-deficient mice had normal swimming performance and no difficulty maintaining their balance. **A,B**. $\alpha_{1D}^{-/-}$ mice are shown performing a swim test in a 37°C water bath and balancing on a stationary cylinder. **C**. The times taken to swim to a target (a dry platform) and to remain on the stationary and rotating cylinder (5 rpm) are illustrated in the histogram. Seven animals from each genotype were tested. The mean of 10 trials for each animal is reported. The mean values for the swim test were as follows (in seconds): $\alpha_{1D}^{+/+}$, = 130 ± 13; $\alpha_{1D}^{-/-}$, $\overline{XX}$ = 132 ± 15 ($n = 7$) $p = 0.3$, NS, and the means values for the balance test were (in seconds): $\alpha_{1D}^{+/+}$, $\overline{X}$ = 85 ± 8; $\alpha_{1D}^{-/-}$, $\overline{X}$ = 87 + 8 ($n = 7$) $p = 0.3$, NS. To eliminate fatigue factor, each trial was separated by a 10-min rest period. No reward was given to the animals during or after the test.

$\alpha_{1D}^{-/-}$ cochlea was a marked reduction in the number of neurons and myelinated fibers in some regions of the spiral ganglion (Fig. 4E, F). These results are consistent with data from ultrastructural analysis of the inner ear of a mouse model similar to one used in this study (Glueckert et al. 2003).

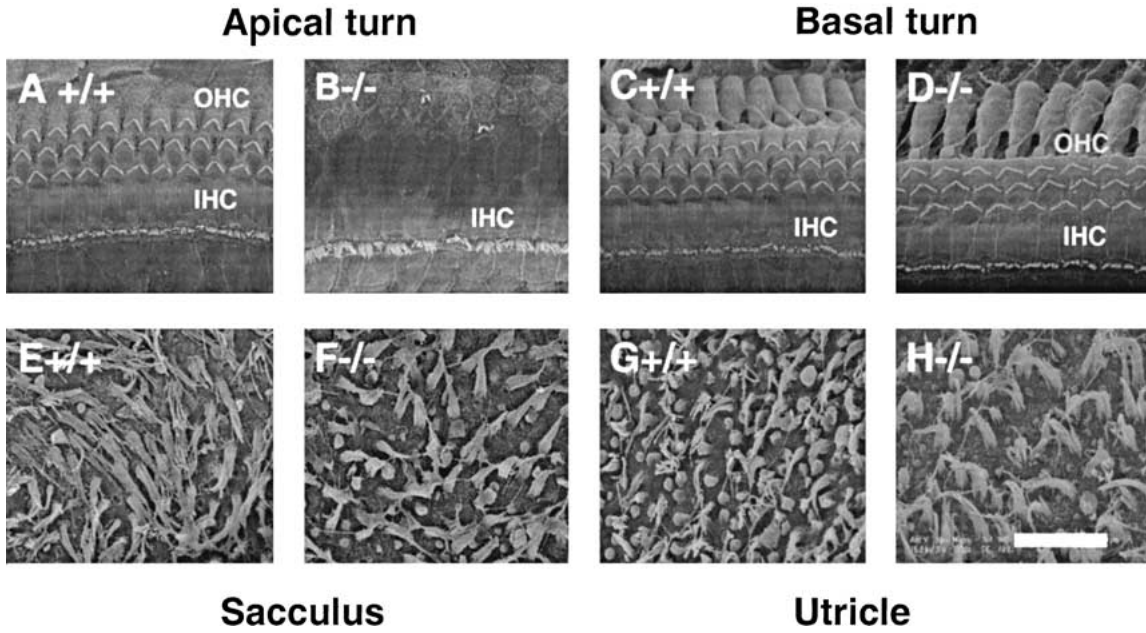

FIG. 3. Scanning electron micrographs of apical (**A,B**) and basal (**C,D**) cochleae of $\alpha_{1D}^{+/+}$ and $\alpha_{1D}^{-/-}$ mice showing robust loss of hair bundles at the apical turn of the mutant cochlea. The basal turn OHCs of $\alpha_{1D}^{-/-}$ mice appear normal (**D**) and are indistinguishable from the wild-type (**C**). In contrast to the morphology of the apical turn of the mutant cochlea in which OHCs are devoid of hair bundles, the saccule (**E,F**) and utricle (**G,H**) of the mutant mice have intact hair bundles. Scale bar: **A–H**, 10 μm.

In agreement with the scanning electron microscopy of the vestibular system from $\alpha_{1D}^{-/-}$ and $\alpha_{1D}^{+/+}$ mice, light microscopy analyses of sections of the saccule (Fig. 5A, D) and cristae ampullaris (Fig. 5C, F) revealed no apparent histopathology. Hair cells, supporting cells, and the innervation of the epithelia in the wild-type and mutant mice appear normal. The otolithic membrane and its associated otoconia were present above the macula in each compartment.

$\alpha_{1D}^{-/-}$ mice yielded little or no DPOAEs at low frequencies compared with $\alpha_{1D}^{+/+}$ and their $\alpha_{1D}^{+/-}$ littermates. However, at 20–48 kHz, $\alpha^{1D-/-}$ mice produced low but moderate-level DPOAEs that were not different from distortion products from the $\alpha_{1D}^{+/+}$ and $\alpha_{1D}^{-/+}$ mice (Fig. 6). These results suggest that the etiology of hearing deficits in $\alpha_{1D}^{-/-}$ mice may result entirely from OHC malfunction.

Whole-cell Ba^{2+} currents in cochlear and utricular hair cells

A major portion of whole-cell Ca^{2+} currents in hair cells is derived from the α_{1D} dihyropyridine-sensitive Ca^{2+} channels (Kollmar et al. 1997a; Zidanic and Fuchs 1995), consistent with the possibility that α_{1D} Ca^{2+} channel deficiency might cause deafness and imbalance. Whole-cell Ba^{2+} currents (I_{Ba}) were measured in 1 mM Ba^{2+} from IHCs and OHCs from the apical and basal turns of the cochlea (P1–2) by suppressing outward K^+ currents with TEA, Cs^+, and NMG (see Methods section). The mean peak I_{Ba} recorded immediately after establishing whole-cell configuration was 175 ± 30 pA (n = 35), followed by a rapid (~45 s) rundown to ~115 + 15 pA (n = 35) where it stabilized. Only data from cells that showed stable recordings after 1.5 min of establishing whole-cell configuration were reported. In addition, the effects of nimodipine were documented after 1.5 min of application. These criteria were extremely important in establishing and disentangling current rundown from drug-induced effects on the I_{Ba} currents in hair cells. The I_{Ba} recorded from IHCs and OHCs was reduced by the application of 20 μM nimodipine. The passive properties of the cells were monitored and cells with significant alterations of the input resistance were voided (Rodriguez–Contreras and Yamoah 2001). Representative traces of I_{Ba} recorded from IHCs and OHCs from $\alpha_{1D}^{+/+}$ mice are shown in Figure 7A. The whole-cell currents were activated from a holding potential of −60 mV to a test potential of −10 mV. The effects of nimodipine on I_{Ba} (Fig. 7A) from the cochlear apical turn in $\alpha_{1D}^{+/+}$ mice included a different level of expression of a non-L-type current [IHC control peak current: $\overline{X}$ = −125 ± 10 pA (n = 9); nimodipine: $\overline{X}$ = −19 ± 2 pA (n = 9), a reduction of ~85% of the whole-cell current; OHC control peak current: $\overline{X}$ = −105 ± 5 pA (n = 7); nimodipine: $\overline{X}$ = −4.0 ± 0.5 pA (n = 7), a reduction of ~96% of the whole-cell current]. The current–voltage relationship shown in Figure 7B re-

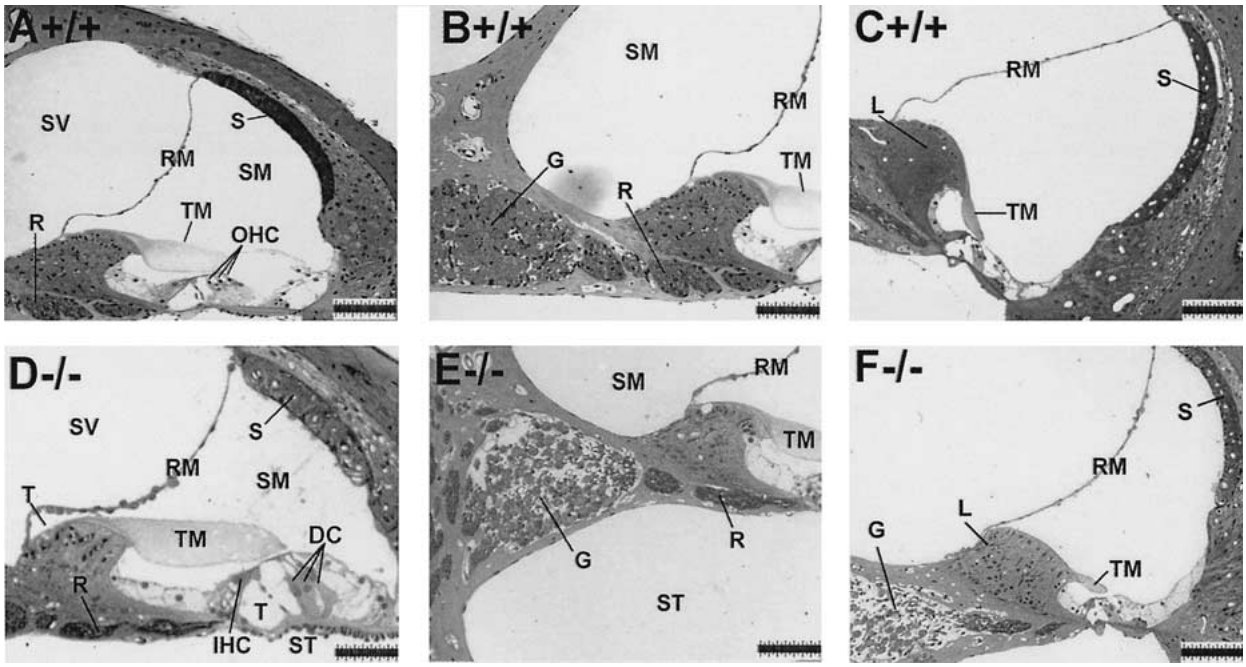

FIG. 4. Light micrographs of cross-sections of the cochlear duct from 6-week-old $\alpha_{1D}^{+/+}$ (**A–C**) and $\alpha_{1D}^{-/-}$ (**D–F**) mice. Reissner's membrane (RM) separating the scala media (SM) and scala vestibuli (SV) in both the wild-type and the mutant cochlea remain intact (**A–F**). Normal histology of the wild-type mouse shows apex (**A**) and base (**C**) for comparison. IHCs and OHCs are identifiable at the apex and base of the cochlea in $\alpha_{1D}^{+/+}$ (**A,C**). Shown in **B** are densely packed cells in the spiral ganglion. Although the cell bodies of OHCs at the apex can be seen in the $\alpha_{1D}^{-/-}$, the hair bundles were absent in the serial sections of the cochlea. More severely affected regions at the apex show fewer identifiable OHCs. However, the IHCs at the apex remain relatively intact in the mutant (**D**). OHCs and IHCs at the base of wild-type and mutant cochlea were normal. Schwann cells and myelinated nerve fibers that fill Rosenthal's canal (R) in the modiolus remain intact in both $\alpha_{1D}^{+/+}$ and $\alpha_{1D}^{-/-}$ cochlea. Spiral ganglion (G) neuronal cell bodies were reduced in number in some mutants (**E,F**). Analysis of random cell counts shows that neuronal cell bodies in **G** were 20 less in $\alpha_{1D}^{-/-}$ compared with $\alpha_{1D}^{+/+}$. Otherwise, the typical architecture of the organ of Corti remains intact in both the wild-type and mutant mice. L, S, SM, ST, SV, T, DC, and TM respectively denote limbus, stria vascularis, scala media, scala tympanic, scala vestibuli, tunnel of Corti, Deiters' cells, and tympanic membrane. Scale bar: 90 μm in **A**, 75 μm in **B–F**.

vealed the presence of a residual current resistant to nimodipine block, consistent with reports that demonstrate the presence of non-L-type Ca^{2+} channels in hair cells (Platzer et al. 2000; Rodriguez and Yamoah 2001). In contrast to IHCs, OHCs that were sampled at the apical turn of the cochlea expressed disproportionately increased levels of nimodipine-sensitive currents (upper right panel, Fig. 7A). In addition, the peak current density of IHCs (26.7 pA/pF) was ~1.5 times larger than in OHCs (16.7 pA/pF) at the apical turn of the cochlea. As shown in Figure 7A, whole-cell inward currents recorded from IHCs of the apical cochlear turn of $\alpha_{1D}^{-/-}$ mice, using 1 mM Ba^{2+} was the charge carrier, reliably revealed the presence of currents that were insensitive to Bay K (10 μM), in accordance with the expression of a non-L-type current [control peak current: $\overline{X} = -26 \pm 4$ pA ($n = 6$); Bay K: $\overline{X} = -25 \pm 5$ pA ($n = 7$); $p = 0.9$, NS]. However, the lack of appreciable current in OHCs at the apical turn in $\alpha_{1D}^{-/-}$ mice [<5 pA ($n = 6$), Fig. 7A, B] suggested that the L- and non-L-type channels may be expressed differentially in the cochlea. To determine whether such differential expression of Ca^{2+} currents occurs along the longitudinal axis of the cochlea, we analyzed the current density (ratio of the peak current/cell capacitance: pA/pF) of I_{Ba} from IHCs and OHCs found in the basal turn of the cochlea. Application of nimodipine reduced I_{Ba} from hair cells at the basal turn of the cochlea from $\alpha_{1D}^{+/+}$ mice by ~80% [control peak current density in IHCs (pA/pF): $\overline{X} = -24.2 \pm 4.3$ ($n = 6$); nimodipine: $\overline{X} = -4.6 \pm 2.1$ ($n = 6$); $p < 0.01$; control peak current density in OHCs: $\overline{X} = -13.8 \pm 2.5$ pA ($n = 7$); nimodipine: $\overline{X} = -3.5 \pm 1.8$ ($n = 7$); $p < 0.01$]. Recordings from hair cells at the basal turn of the cochlea of $\alpha_{1D}^{-/-}$ mice were consistent with the presence of ~20% of non-L-type currents in IHCs [control peak current density in IHCs (pA/pF): $\overline{X} = -4.8 \pm 2.1$; Bay K: $\overline{X} = -4.7 \pm 2.4$ ($n = 6$); $p = 0.5$, NS]. Moreover, unlike the OHCs in the apical turn of the cochlea, the non-L-type current was substantial [control peak current density in OHCs (pA/pF): $\overline{X} = -3.5 \pm 1.2$; Bay K: $\overline{X} = -3.6 + 0.8$ ($n = 7$); $p = 0.3$, NS]. The group data for the current density and the effects of nimodipine on IHCs and OHCs from the basal cochlea are shown in Figure 7C. Thus, differential expression

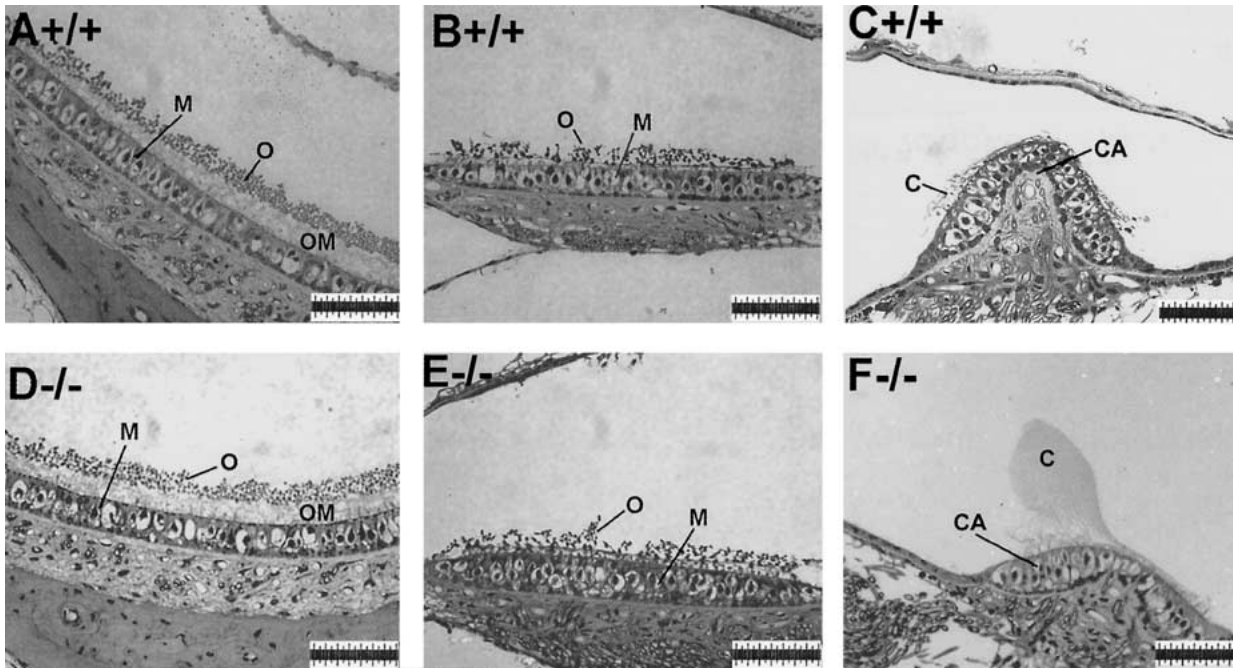

FIG. 5. In the saccule (**A**,**D**) and utricle (**B**,**E**) of the $\alpha_{1D}^{+/+}$ and $\alpha_{1D}^{-/-}$ mice, the otoconia (O) are embedded in the otolithic membrane (OM) overlying the neuroepithelium of the macula (M). Tufts of hair bundles and corresponding cell bodies are identifiable in the mutant and wild-type saccule and utricle. The structure of the ampulla of the semicircular ducts of $\alpha_{1D}^{+/+}$ and $\alpha_{1D}^{-/-}$ (**C**,**F**, respectively) and the gelatinous cupula (C) overlying the crista

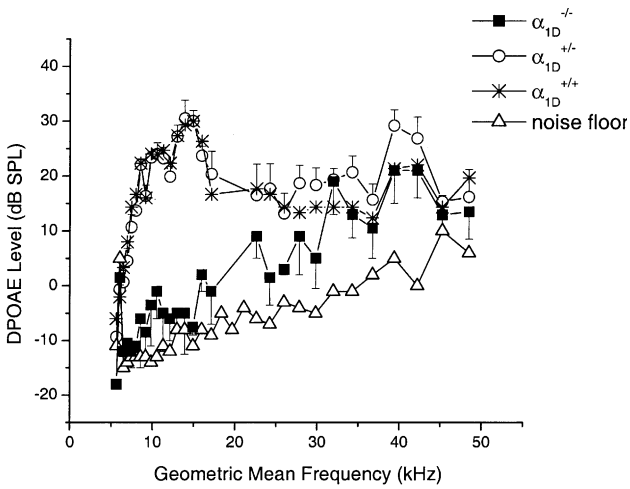

FIG. 6. Mean DP-grams for 6 weeks $\alpha_{1D}^{+/+}$, $\alpha_{1D}^{+/-}$, and $\alpha_{1D}^{-/-}$ ($n = 6$) were tested measuring the levels of the 2 $f_1 - f_2$ DPOAE over a geometric-mean frequency range from 5.6 to 48.5 kHz, using an f_2/f_1 of 1.25, and primary tone stimuli at $L_1 = L_2 = 65$ SPL. Clearly, $\alpha_{1D}^{-/-}$ mice yielded no significant DPOAEs at low frequencies (5–15 kHz) compared with $\alpha_{1D}^{+/+}$ and $\alpha_{1D}^{+/-}$ mice. However, at 20–48 kHz, $\alpha_{1D}^{-/-}$ produced modest DPs.

of the Ca^{2+} channels in cochlear hair cells may be prevalent at the apical turn.

We also investigated the effects of the dihydropyridines on utricular hair cells. The effects of nimodipine on I_{Ba} from hair cells from the utricle of $\alpha_{1D}^{-/-}$ mice show that nearly 50% of the current was resistant to the drug [control peak current (pA): $\overline{X} = -107 \pm 11$; nimodipine: $\overline{X} = -52 \pm 16$ ($n = 9$), Fig. 8A, B]. The data were obtained from the peak current elicited at −10 mV. An example of the effect of nimodipine on wild-type utricular hair cells and the effect of Bay K (10 μM) on the mutant I_{Ba} traces is shown in the lower panel of Figure 8A. The data were further corroborated by the measurement of a robust I_{Ba} from utricular hair cells from the $\alpha_{1D}^{-/-}$ mice (62 ± 6 pA; $n = 7$), consistent with the differential expression of Ca^{2+} channel subtypes in hair cells from the vestibule and the cochlea. Thus, deletion of the channel subtype imparts a functional-specific deficiency as opposed to complete disruption of all hair cell activity.

DISCUSSION

$\alpha_{1D}^{-/-}$ mice were generated to better understand the physiological functions of this particular Ca^{2+} channel isoform in hearing and balancing. The most robust feature of the $\alpha_{1D}^{-/-}$ mice was deafness and increased thresholds for audiological response to sound in the heterozygote littermates, which was restricted mainly to low-frequency sounds. A completely unexpected finding was that the hearing loss was not associated with gross structural changes in IHCs, suggesting that α_{1D} Ca^{2+} channels play a minimal role

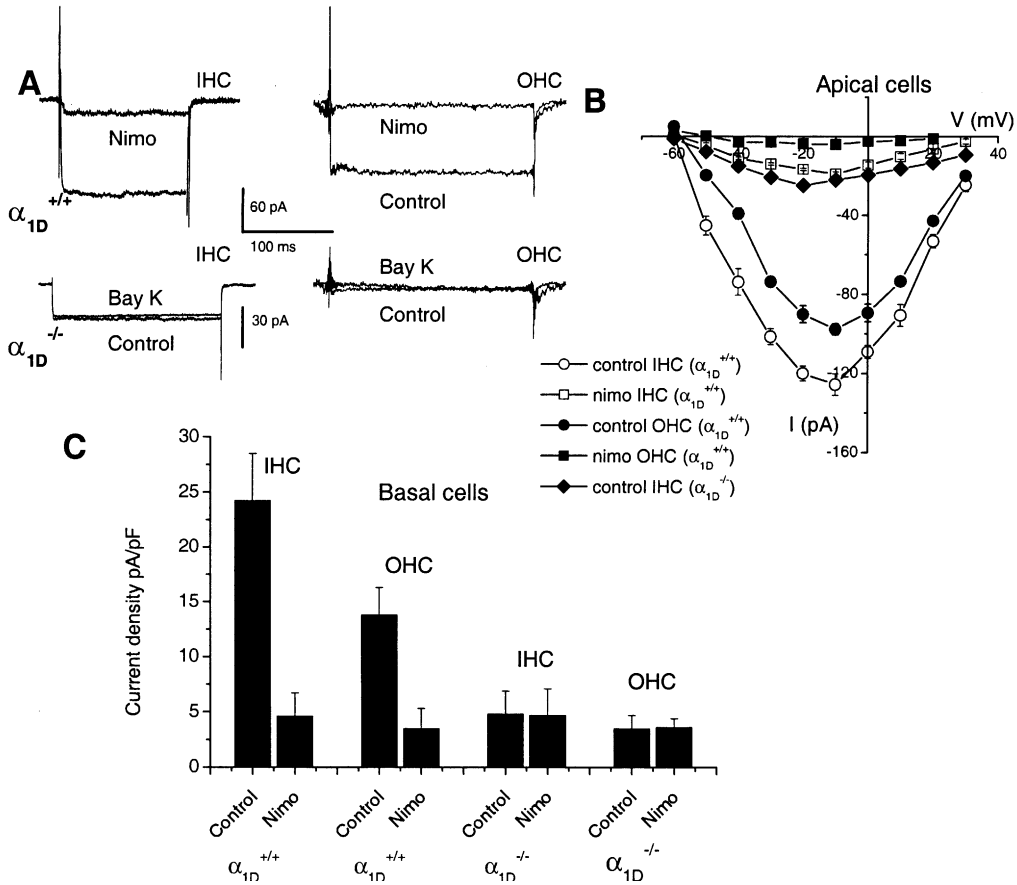

FIG. 7. Inward Ba^{2+} currents through whole-cell Ca^{2+} channels recorded from hair cells in intact cochlea. **A**. Whole-cell Ba^{2+} currents from IHCs at the apical turn of PI wild-type ($\alpha_{1D}^{+/+}$) mice were elicited from a holding potential of −60 mV to a step potential of −10 mV. Only current traces that stabilized after initial current rundown were analyzed and shown. After 90 s and an application of nimodipine (20 μM), the whole-cell Ba^{2+} currents were reduced by ~80 (left upper panel). The right upper panel shows Ba^{2+} current traces recorded from an OHC at the apical turn of the cochlea and of the effect of nimodipine (20 μM) on the current. For OHCs, nimodipine blocked at least 95 of the whole-cell Ba^{2+} currents. The middle panels consist of Ba^{2+} current traces generated from hair cells at the apical cochlear of PI mutant ($\alpha_{1D}^{-/-}$) mice. In contrast to IHCs (left), OHCs (right) in the $\alpha_{1D}^{-/-}$ did not express Ba^{2+}-permeable inward current channels. **B**. Current–voltage relationships of Ba^{2+} currents in hair cells at the apical turn of the cochlea (IHC, $n = 9$; OHC, $n = 7$). C. In contrast to OHCs at the apical turn, there were substantial residual currents following the application of nimodipine (20 μM) on OHCs at the basal turn of the cochlea. Group data of Ba^{2+} current densities shown in a bar graph from IHCs ($n = 6$) and OHCs ($n = 7$) at the basal turn of the cochlea in $\alpha_{1D}^{+/+}$ and $\alpha_{1D}^{-/-}$ mice.

in maintaining IHC morphology. The findings that the OHCs at the apical turn of the cochlea expressed mostly the nimodipine-sensitive Ca^{2+} currents (>95%: α_{1D} Ca^{2+} channels) and that hair cells in this region of the cochlea degenerated in α_{1D}-deficient mice may indicate that Ca^{2+} is required for the maintenance of OHC morphology. Other Ca^{2+} channel subtypes are known to be present in hair cells and they carry a residual current following block by nimodipine. Although this nimodipine-insensitive current in IHCs in $\alpha_{1D}^{-/-}$ mice may sustain the cellular architecture, the current may not be sufficient to mediate adequate neurotransmitter release to confer hearing. In contrast, the results for hair cells in the vestibule indicate that the non-α_{1D} Ca^{2+} channels may be sufficient in maintaining both the structure and functions of the cells. Although gross assessment of the vestibular function suggested that the $\alpha_{1D}^{-/-}$ mice have no vestibular defect, a more direct diagnosis of vestibular function may be required. Nonetheless, we infer that differential expression of diverse Ca^{2+} channel subtypes in hair cells of the inner ear helps explain the balance and auditory phenotypes of the α_{1D} Ca^{2+} channel-deficient mice.

Hearing in vertebrates requires the precise synchronization of cochlear IHC activity and the auditory nerve. Previous studies have shown that the kinetics and voltage-dependent activation properties of the L-type channels in mammalian cochlear IHCs and hair cells from other vertebrates may suffice to confer both the tonic and phasic Ca^{2+}-dependent release of neurotransmitters (Hudspeth 1989; Zidanic and Fuchs 1995; Martinez–Dunst et al. 1997; Moser and Beutner 2000; Beutner et al. 2001). How-

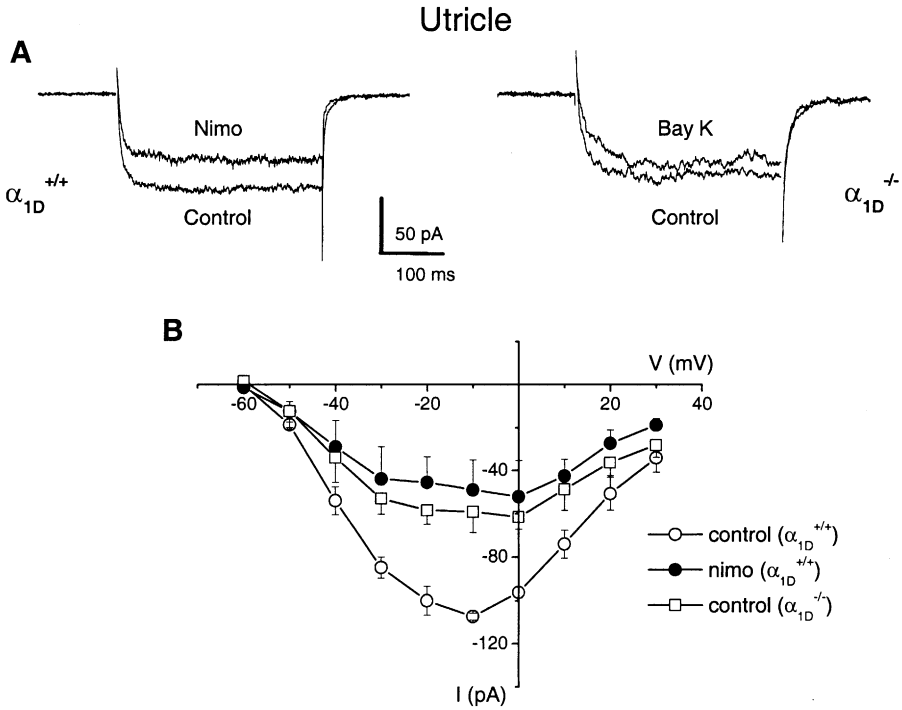

FIG 8. Inward Ba^{2+} currents through whole-cell Ca^{2+} channels recorded from hair cells in intact utricle. **A**. Approximately 50 of the whole-cell Ba^{2+} currents of utricular hair cells from $\alpha_{1D}^{+/+}$ mice were sensitive to 20 μM nimodipine. As expected, Ba^{2+} currents of hair cells from the utricle of $\alpha_{1D}^{-/-}$ mice (right panel) were insensitive to Bay K (10 μM). **B**. Current–voltage relationships of Ba^{2+} currents from utricular hair cells (n = 9) of $\alpha_{1D}^{+/+}$ and $\alpha_{1D}^{-/-}$ mice.

ever, recent reports have demonstrated that hair cells in lower vertebrates and mammals do express nimodipine-insensitive Ca^{2+} currents (Su et al. 1995; Martini et al. 2000; Platzer et al. 2000; Rodriguez–Contreras and Yamoah 2001). Although the functions of the non-L-type current remain unclear, their voltage-dependent properties suggest a possible function in tonic release of neurotransmitters (Martini et al. 2000; Rodriguez–Contreras and Yamoah 2001). Measurements of hair cell capacitance as an index for exocytotic release of neurotransmitters from hair cells have shown that the nimodipine-sensitive component of the whole-cell Ca^{2+} (L-type) current plays a marked role in phasic neurotransmitter release. Moreover, the functions of non-L-type current may be obscured by its baseline activity and minimal contribution toward the hair cell Ca^{2+} current (Moser and Beutner 2000; Spassova et al. 2001). A more sensitive method for resolving neurotransmitter release, such as postsynaptic recordings, may be required to determine the contribution of the non-L-type current (von Gersdorff et al. 1998; Spassova et al. 2001). Nonetheless, the *in vivo* and *in vitro* results presented strongly indicate that the α_{1D} Ca^{2+} channel is critically required for hair cell functioning and hearing.

Our findings on the properties and expression patterns of the L-type current in IHCs and OHCs are consistent with previous reports using hair cells from frog (Hudspeth and Lewis 1988; Su et al. 1995; Smotherman and Narrins 1999; Rodriguez–Contreras and Yamoah 2001), chick (Kimitsuki et al. 1994; Zidanic and Fuchs 1995), and guinea pig (Rennie and Ashmore 1991). The activation threshold (~50 mV), rapid onset (time-to-peak = ~1 ms), and slow inactivation of the nimodipine-sensitive current are reminiscent of those previously described in cochlear and vestibular hair cells. Similar to whole-cell Ca^{2+} currents in other hair cells, the expression pattern is heterogenous. Our observations add significantly new findings, which demonstrate that for OHCs, the contribution of the non-L-type current toward the total Ca^{2+} current increases along the axis of the cochlea with cells at the apical turn expressing little non-α_{1D} channel current and those at the basal turn expressing ~15% of the non-L-type current. Because OHCs at the basal turn of the cochlea have sufficient non-L-type current and retain their gross cellular morphology and because the cells at the apical turn virtually lack the non-L-type Ca^{2+} current in the $\alpha_{1D}^{-/-}$ mice, hence having little Ca^{2+} influx leading to OHC degeneration, the possibility that the non-L-type Ca^{2+} channel in hair cells may play housekeeping roles in addition to other cell-specific functions is raised. Furthermore, synaptic connections between OHCs and afferent nerve terminals are physiologically silent (Robertson and Gummer 1985). Thus, the L-type current is not expected to play an obvious role in neurotransmitter release. Moreover, there are a plethora of physiological activities in cells which require Ca^{2+} as a second messenger (Fuchs 1996).

At the macroscopic level, the results of the present studies are similar to recent data from α_{1D} null mutant mice published by Platzer et al. (2000). However,

our extension of the previous studies revealed important differences at the microscopic level. Serial sectioning of the entire cochlea at the light microscope level and scanning electron microscopy clearly showed that only the OHCs at the apical turn of the cochlea degenerate in 5–7-week-old $\alpha_{1D}^{-/-}$ mice. This is in sharp contrast to an earlier report that both IHCs and OHCs degenerated after P14 (Platzer et al. 2000). Although the previous report may reflect genuine differences between the two models, it is likely that evaluation of different planes of sections without complete serial reconstruction led to the earlier results (Platzer et al. 2000). Thus, our findings confirm the earlier report that α_{1D} Ca^{2+} channel knockout mice have hearing impairment despite apparent normal IHC morphology. We have extended the scope of these studies to demonstrate that with the exception of OHCs at the apical turn of the cochlea which degenerate, cochlear hair cells do remain intact in the $\alpha_{1D}^{-/-}$ mice.

Finally, neurotransmitter release by hair cells onto afferent nerve terminals of the vestibular nerve is mediated by Ca^{2+} entry via presynaptic VGCCs. Although the nimodipine-sensitive Ca^{2+} current contributes substantially to the VGCC in vestibular hair cells (Hudspeth and Lewis 1988; Prigioni et al. 1992; Martini et al. 2000; Rispoli et al. 2001), our behavioral and electrophysiological analyses of the vestibular system of the $\alpha_{1D}^{-/-}$ mice show that in addition, there is a non-nimodipine-sensitive current. In contrast to the auditory system, the vestibular hair cells employ multiple VGCCs that mediate neurotransmitter release to ensure proper balance. Hair cells in both the cochlea and the vestibule share common morphological and functional traits that are usually difficult to disentangle. Thus, the differential expression and functions of Ca^{2+} channel isoforms in vestibular and cochlear hair cells will ultimately constitute an invaluable functional and molecular biological tool to study the two systems in isolation.

ACKNOWLEDGMENTS

We thank Dr N. Chiamvimonvat and members of our laboratory for their constructive comments on the manuscript. This work was supported by grants to ENY from the NIH (R01 DC03828, DC04512).

REFERENCES

BEUTNER D, VOET T, NEHER E, MOSER T. Calcium dependence of exocytosis and endocytosis at the cochlear inner hair cell afferent synapse. Neuron 29:681–690, 2001.

ERTEL AA, CAMPBELL KP, HARPOLD MM, HOFMANN F, MORI Y, PEREZ–REYES E, SCHWARTZ A, SNUTCH TP, TANABE T, BIRNBUAMER L, TSIEN WA, CATTERALL WA. Nomenclature of voltage-gated calcium channels. Neuron 25:533–535, 2000.

FLAGELLA M, CLARKE LL, MILLER ML, ERWAY LC, GIANELLA RA, KRAMER J, DUFFY JJ, DOESTCHMAN T, LORENZ JN, YAMOAH EN, CARDELL GE, SHULL GE. Mice lacking the basolateral $Na^+/K^+/2Cl^-$ cotransporter have impaired intestinal chloride secretion and are profoundly deaf. J. Biol. Chem. 274:26946–26955, 1999.

FUCHS PA. Synaptic transmission at vertebrate hair cells. Curr. Opinion Neurobiol. 6:514–163, 1996.

GLUEKERT R, WIETZORREK G, KAMMEN–JOLLY K, SCHOLTZ A, STEPHAN J, STRIESSNIG J, SCHROTT–FISHER A. Role of class D L-type Ca^{2+} channels for cochlear morphology. Hear. Res. 178:95–105, 2003.

GREEN GE, KHAN KM, BEISEL DW, DRESCHER MJ, HARTFIELD JS, DRESCHER DJ. Calcium channel subunits in the mouse cochlea. J. Neurochem. 67:37–45, 1996.

HALL JD, BETARBET S, JARAMILLO F. Endogenous buffers limit the spread of free calcium in hair cells. Biophys. J. 73:1243–1252, 1997.

HENRY KR, CHOLE RA. Genotypic differences in behavioral, physiological and anatomical expressions of age-related hearing loss in the laboratory mouse. Audiology 19:369–383, 1980.

HOLT JR, COREY DP, EATOCK EA. Mechanoelectrical transduction and adaptation in hair cells of the mouse utricle, a low-frequency vestibular organ. J. Neurosci. 17:8739–8748, 1997.

HUDSPETH AJ. How the ear's works work. Nature 34:397–404, 1989.

KIMITSUKI T, NAKAGAWA T, HIASAHI K, KOMUNE S, KOMIYAMA S. Single channel recordings of calcium currents in chick cochlear hair cells. Acta Otolaryngol. 114:144–148, 1994.

KOLLMAR R, FAK J, MONTGOMERY LG, HUDSPETH AJ. Predominance of the α_{1D} subunit in L-type voltage-gated Ca^{2+} channels of hair cells in the chicken's cochlea. Proc. Natl. Acad. Sci. USA 94:14883–14888, 1997a.

KOLLMAR R, FAK J, MONTGOMERY LG, HUDSPETH AJ. Hair cell-specific splicing of mRNA for the α_{1D} subunit of voltage-gated Ca^{2+} channels in the chicken's cochlea. Proc. Natl. Acad. Sci. USA 94:14889–14893, 1997b.

KOZEL PJ, FRIEDMAN RA, ERWAY LC, YAMOAH EN, LUI LH, RIDDLE T, DUFFY JJ, DOETSCHMAN T, MILLER ML, CARDELL EL, SHULL GE. Balance and hearing deficits in mice with a null mutation in the gene encoding plasma membrane Ca^{2+}-ATPase isoform 2*. J. Biol. Chem. 273:18693–18696, 1998.

LEWIS RS, HUDSPETH AJ. Voltage- and ion-dependent conductances in solitary vertebrate hair cells. Nature 304:238–541, 1983.

LIN Z, HAUS S, EDGERTON J, LIPSCOMBE D. Identification of functionally distinct isoforms of the N-type Ca^{2+} channel in rat sympathetic ganglia and brain. Neuron 18:153–166, 1997.

LOPEZ I, ISHIYAMA G, ISHIYAMA A, JEN JC, LIU F, BALOH RW. Differential subcellular immunolocalization of voltage-gated calcium channel α1 subunits in the chinchilla cristae ampullaris. Neuroscience 92:773–782, 1999.

MARTINEZ-DUNST C, MICHAELS RL, FUCHS PA. Release sites and calcium channels in hair cells of the chick's cochlea. J Neurosci. 17:9133–9144, 1997.

MARTINI M, ROSSI ML, RUBBINI G, RISPOLI G. Calcium currents in hair cells from semicircular canals of the frog. Biophys. J. 78:1240–1254, 2000.

MOSER T, BEUTNER D. Kinetics of exocytosis and endocytosis at the cochlear inner hair cell afferent synapse of the mouse. Proc. Natl. Acad. Sci. USA 97:883–888, 2000.

NAMKUNG Y, SKRYPNYK N, JEONG M-J, LEE LT, LEE M-S, KIM H-L, CHIN P-G, SUH P-G, KIM S-S, SHIN H-S. Requirement for the L-type Ca^{2+} channel 1D subunit in postnatal pancreatic β cell generation. J. Clin. Invest. 108:1015–1022, 2002.

PLATZER J, ENGEL J, SCHROTT-FISCHER A, STEPHAN K, BOVA S, CHEN H, ZHENG H, STRIESSNIG J. Congenital deafness and sinoatrial node

dysfunction in mice lacking class D L-type Ca^{2+} channels. Cell 102:89–97, 1995.

PRIGIONI I, MASETTO S, RUSSO G, TAGLIETTI V. Calcium currents in solitary hair cells isolated from frog crista ampullaris. J. Vestib. Res. 2:31–39, 1992.

RENNIE KJ, ASHMORE AF. Ionic currents in isolated vestibular hair cells from guinea-pig crista ampullaris. Hear. Res. 51:279–292, 1991.

RISPOLI G, MARTINI M, ROSSI ML, MAMMANO F. Dynamics of intracellular calcium in hair cells isolated from the semicircular canal of the frog. Cell Calcium 30:131–140, 2001.

ROBERTS MW, JACOBS AR, HUDSPETH AJ. Co-localization of ion channels involved in frequency selectivity and synaptic transmission at presynaptic active zones of hair cells. J. Neurosci. 10:3664–3684, 1990.

ROBERTSON D, GUMMER M. Physiological and morphological characterization of efferent neurons in the guinea cochlea. Hear. Res. 20:63–77, 1985.

RODRIGUEZ–CONTRERAS A, YAMOAH EN. Direct measurement of single-channel Ca^{2+} currents in bullfrog hair cells reveals two distinct channel subtypes. J. Physiol. (Lond.) 534:669–689, 2001.

RODRIGUEZ–CONTRERAS A, YAMOAH EN. Ca^{2+} transport properties and determinants of anomalous mole fraction effects of single voltage-gated Ca^{2+} channels in hair cells from bullfrog saccule. J. Physiol. (Lond.) 538:729–745, 2002.

RÜSCH A, EATOCK RA. A delayed rectifier conductance in type I hair cells of the mouse utricle. J. Neurophysiol. 76:995–1004, 1996.

SMITH AB, CUNNANE TC. Multiple calcium channels control neurotransmitter release from rat postganglionic sympathetic nerve terminals. J Physiol. (Lond.) 499:341–349, 1997.

SMOTHERMAN MS, NARINS PM. The electrical properties of auditory hair cells in the frog amphibian papilla. J. Neurosci. 19:5275–5292, 1999.

SOLATOV NM, BOURON A, REUTER H. Different voltage-dependent inhibition by dihydropyridines of human Ca^{2+} channel splice variants. J. Biol. Chem. 270:10540–10543, 1995.

SPASSOVA M, EISEN MD, SAUNDERS JC, PARSONS TD. Chick cochlear hair cell exocytosis mediated by dihydropyridine-sensitive calcium channels. J. Physiol. (Lond.) 535:689–696, 2001.

SU Z-L, JIANG SC, GU R, YANG WP. Two types of calcium channels in bullfrog saccular hair cells. Hear. Res. 87(1–2): 62–68, 1995.

TUCKER T, FETTIPLACE R. Confocal imaging of calcium microdomains and calcium extrusion in turtle hair cells. Neuron 15:1323–1335, 1995.

VON GERSDORFF H, SAKABA T, BERGLUND K, TACHIBANA M. Submillisecond kinetics of glutamate release from sensory synapse. Neuron 21:1177–1188, 1998.

WU L-G, WESTENBROEK RE, BORST JGG, CATTERALL WA, SAKMANN B. Calcium channel types with distinct presynaptic localization couple differentially to transmitter release in single calyx-type synapses. J. Neurosci. 19:726–736, 1999.

XIANG M, GAN L, LI D, CHEN Z-Y, ZHOU L, O'MALLEY BW Jr, KLEIN W, NATHANS J. Essential role of POU-domain factor Brn-3c in auditory and vestibular hair cell development. Proc. Natl. Acad. Sci. USA 94:9445–9450, 1997.

YAMOAH EN, GILLESPIE PG. Phosphate analogs block adaptation by hair cells by inhibiting adaptation-motor force production. Neuron 17:523–533, 1996.

ZIDANIC M, FUCHS PA. Kinetic analysis of barium currents in chick cochlear hair cells. Biophys. J. 68:1323–1336, 1995.